International Journal of Science and Research (IJSR)
ISSN (Online): 2319-7064
Index Copernicus Value (2013): 6.14 | Impact Factor (2015): 6.391

Fabrication of Encapsulated HEC Silver Gold Nanocomposite Films for Improved Antimicrobial Activity

Alvakonda Narayanamma[1], Dr. M. E. Rani[2], K. Mohana Raju[3]

[1, 3]Synthetic Polymer Laboratory, Department of Polymer Science & Technology
Sri Krishnadevaraya University, Anantapur-515055, Andhra Pradesh, India

[2]Professor, Department of Chemistry, Rayalaseema University, Kurnool, Andhra Pradesh, India

Abstract: ***The presence of silver-gold nanoparticles in the HEC film is confirmed by UV-Vis spectroscopy, Fourier Transform Infrared (FTIR) spectroscopy and X-ray Diffraction (XRD) analysis. The Scanning Electron Microscopic (SEM) images provide the information embedded silver-gold nanoparticles throughout the films. In addition, the formed silver-gold nanoparticles have an average particle size of gold and silver are estimated to be about 5 and 8 nm observed by Transmission Electron Microscopy (TEM). The anti-microbial activity of the silver –gold nanoparticle films have demonstrated significant effects against Escherichia coli (E. coli) and Bacillus. The present study illustrates novel antimicrobial films which are potentially useful in treating infections.***

Keywords: Silver and gold Nanoparticles, HEC, biomedical applications, antimicrobial activity, bi-metallic, films

1. Introduction

Nanotechnology deals with structures ranging from approximately 1 to 100nm in at least one dimension. Bulk chemicals have specific physicochemical characteristics effect is attributed to high surface area to volume ratio, which potentially results in high reactivity. Because of these, the use of these substances in nanoform may have advantages over the use of bulk chemicals.

The current trend in nanotechnology research is to use biocompatible or biological friendly polymers which can provide reduction and stabilization functions in the preparation of silver –gold nanoparticles.

Natural polymers like starch [1, 2–8], chitosan [9], and cellulose [10–12] were reported to stabilize silver –gold nanoparticles. Nanocomposite films possessed good mechanical properties and thermal stability, both of which are comparable to the pure cellulose films.

Films based on biopolymers function as barriers against moisture, oxygen, aroma flavor as well as oil and have future applications [13]. In addition have supports for antimicrobial, nutritional and antioxidant substances.

Bimetallic nanocomposite hydrogels form nanocomposite functional materials, comprises a metallic core covered with a shell of another metal. Durango *et al*. [14] developed edible antimicrobial films using yarn starch and chitosan and effective against S. enteritidis. Tripathi *et al.* [15] prepared chitosan- PVA blend films for food packaging applications and they have also shown to possess antimicrobial activity against food pathogenic bacteria Metal nanoparticles (either Ag or Au) do not act via cell receptors to kill the micro organisms.

Hydroxyethyl cellulose (HEC) is a derivative of cellulose with excellent water solubility and biocompatibility. It is used in many biotechnological, biophysical, and Industrial fields. In Hydroxyethyl cellulose (HEC) the ethyl group replaces one or more of three hydroxyl groups, which are present in each glucopyranoside. Hydroxyl groups on the HEC backbone reduce the silver metal ions to florets of 5 - 10 µM and acts as a capping agent. Because of the existence of abundant reactive –OH groups on the HEC chains, HEC is liable to be modified to derive new materials with improved properties.

Hydroxyethyl cellulose (HEC) reduces the Ag^{+}-Au^{3+} ions to Ag^{0}-Au^{0} nanoparticles. Hydroxyethyl cellulose (HEC), an ecofriendly polymer, is used as both reducing and stabilizing agents in the synthesis of stable silver-gold nanoparticles. Hydroxyethyl cellulose (HEC) products are water-soluble polymers that thicken, form films, exhibit pseudoplastic solution behavior, tolerate salts and retain water.

2. Materials

HydroxyethylCellulose(HEC),NaOH,N,N^{1}-methylenebisacrylamide(MBA),Ammonium persulphate(APS) and N,N,N^{1},N^{1}-teramethylethylenediamine (TMEDA), silver nitrate(AgNO3), gold chloride ($H.AuCl_4$. XH2O) were purchased from SD Fine Chemicals (Mumbai, India). Double distilled water was used throughout the investigations for the preparation of all solutions.

2.1 Preparation of HEC films

1g, 2g, 3g of HEC powder was dissolved in 100 ml of 0.25N NaOH solution and stirred for 6 h. To this solution additionally 6 mM of 1% MBA and 6 mM of APS were added for strong network. The reactant solution was transferred immediately onto a Teflon sheet covered glass plate (dimensions: 100 mm length x 100 mm width x 3 mm height) and dried at 25°C for 12 h. Finally this film was cut into the required length and width for further studies. The

Licensed Under Creative Commons Attribution CC BY

film codes and the corresponding feed composition are listed in table-1.

2.2 Preparation of HEC nanocomposite films

1g, 2g, 3g of HEC was dissolved in 100 ml 0.25N NaOH solution and stirred for 6 h. To this, $AgNO_3$ solution (200 mg/10 ml distilled water), 6 mM of MBA solution and 6 mM of APS solution were added at 25°C. This solution was kept in the sunlight for 1 h. The colorless solution started turning to red, then brown and brownish indicating the formation of AgNPs. The solution was then poured onto Teflon covered glass plates and dried as explained earlier. Finally, the dried film was cut into the required size for further studies. The gold nanoparticles are prepared as same procedure.

2.3 Preparation of Ag- Au Bi-metallic HEC nanocomposite films

1g, 2g, 3g of HEC was dissolved in 100 ml 0.25N NaOH solution and stirred for 6 h. To this $AgNO_3$ solution (200 mg/10 ml distilled water), and 2 mL of gold chloride (5 mM) aqueous solutions,), 6 mM of MBA solution and 6 mM of APS solution were added at 25°C. This solution was kept in the sunlight for 1 h and the solution turned into brownish black color indicating the formation of nanoparticles. The solution was then poured onto Teflon covered glass plates and dried as explained earlier. Finally, the dried film was cut into the required size for further studies.

2.4 Swelling studies

Dried films were swollen in (100 ml) phosphate buffer (pH 7.4) solution at 25°C. The weight of swollen films was measured at equilibrium swelling after removing the surface solution with filter paper. Swelling ratio (Q) was calculated as follows: $Q = \frac{W_e}{W_d}$, where W_e is the weight of the swollen film at equilibrium and W_d is the dry weight of the film.

Table 1: Feed Compositions of HEC based films Preparation Conditions

Sample code	HEC (gm)	$AgNO_3$ (mg)	$HAuCl_4$ (ml)	MBA (ml)	APS (ml)
HEC_1	1	---	---	6	6
HEC_2	2	---	---	6	6
HEC_3	3	---	---	6	6
$(HEC+Ag)_1$	1	100	---	6	6
$(HEC+Ag)_2$	2	100	---	6	6
$(HEC+Ag)_3$	3	100	---	6	6
$(HEC+Au)_1$	1	---	2	6	6
$(HEC+Au)_2$	2	---	2	6	6
$(HEC+Au)_3$	3	---	2	6	6
$(HEC+Ag\text{-}Au)_1$	1	100	2	6	6
$(HEC+Ag\text{-}Au)_2$	2	100	2	6	6
$(HEC+Ag\text{-}Au)_3$	3	100	2	6	6

The swelling ratios of film samples were measured at ambient temperature using a gravimetric method. The dried films were immersed in a 50 ml beaker containing double distilled water until their weight becomes constant. The films were then removed from water and their surfaces were blotted with filter paper before being weighed. Furthermore, the swollen films were treated with $AgNO_3$ via a green process. The swelling ratio or swelling capacity (Sg/g) of the film developed and their nanocomposites were calculated using the equation 1:

$$Swellingr\ ratio : (S_{g/g}) = \frac{(W_s - W_d)}{W_d} \quad (1)$$

where W_s and W_d denote the weight of the swollen film at equilibrium and the weight of the dry film, respectively. The data provided is an average value of 4 individual sample readings. The swelling studies are presented in the form of graph in Fig.2 in the results & discussion section.

2.5 Characterization

2.5.1 FTIR spectroscopy

To record the FTIR spectra of films, the samples were completely dried in an oven at 40LC for 6 h. The spectra was recorded between 500 and 4000 cm^{-1} on a MB3000 Model, ABB company (Horizon software) FTIR spectrometer (Quebec, Canada) using the KBr disk method. It is used to investigate the surface chemistry of the nanoparticles as polymer-stabilized nanoparticles give IR bands characteristics of the polymer.

2.5.2 UV–Vis spectrophotometer

UV–Vis absorption spectra of the samples were recorded on a Shimadzu 160A model UV–Vis spectrophotometer in the range of 200–700 nm. For this study, 100 mg of silver nanocomposite film was dispersed in 10 ml of distilled water and allowed for 1 day to extract all silver-gold nanoparticles into aqueous phase and these solutions were used for absorption spectra.

2.5.3. Scanning electron microscopy (SEM)

The signals that derive from electron-sample interactions reveal information about the sample including external morphology (texture), chemical composition, and crystalline structure and orientation of materials making up the sample. The morphological ariations of silver-gold nanoparticles were observed.

2.5.4. Transmission electron microscopy (TEM)

The size of the Ag-AuNPs in film network was determined using a Technai F12 TEM (Tokyo, Japan) microscope. For this study, the samples were prepared by placing a drop of aqueous solution of SCMC SNCF on carbon-coated copper grid and subsequently drying in air, before transferring them to the microscope operated at an accelerated voltage of 120 kV. It is used to find out the size of nanoparticles inside the hydrogel nanocomposites.

2.5.5. X-ray diffraction (XRD)

The X-ray diffraction method was used to identify the formation of nanoparticles in the films. The phase changes with increasing diameter of nanoparticles and the crystal structure can be determined with XRD. These measurements were carried out for dried and finely grounded samples on a Rikagu diffractometer (Cu radiation, k = 0.1546 nm) running at 40 kV and 40 mA.

Licensed Under Creative Commons Attribution CC BY

2.5.6. Thermogravimetric analysis (TGA)
The thermal analysis of pristine and Ag-AuNPs loaded films was carried on a SDT Q 600 TGA instrument (T.A. Instruments-water LLC, Newcastle, DE 19720, USA) at a heating rate of 10LC/min in 40–700LC range under a constant nitrogen flow (100 ml/min).

2.5.7. Differential scanning calorimetry (DSC)
Differential scanning calorimetry thermograms of pure Hydroxyethyl cellulose(HEC), Ag-AuNPs loaded film and HEC loaded silver-gold nanocomposite films were recorded using a SDT Q 600 DSC instrument (T.A. Instruments-water LLC, New-castle, DE 19720, USA) at a heating rate of 10LC/min under a constant nitrogen flow (100 ml/min)in the temperature range of 40–450LC.

2.5.8. Antibacterial activity:
The antibacterial activity of the HEC+ Ag^0 –Au^0 nanocomposite HEC film, under study, was investigated by disc method, using the standard procedure described elsewhere (Vimala, Samba Sivudu,Murali Mohan, Sreedhar, & Mohana Raju, 2009; Varaprasad, Vimala,Ravindra, Narayana Reddy, Venkata Subba Reddy, et al., 2011; Varaprasad, Vimala, Ravindra, Narayana Reddy, & Mohana Raju,2011). Nutrient agar medium was prepared by mixing peptone (5.0 g), beef extract (3.0 g) and sodium chloride (NaCl) (5.0 g) in 1000 ml distilled water and the pH was adjusted to 7.0. Finally, agar (15.0 g) was added to the solution. The agar medium was sterilized in a conical flask using Autoclave at a pressure of 6.8 kg (15 lbs) for 30 min. This medium was transferred into sterilized Petri dishes in a laminar air flow chamber (Microfilt Laminar Flow Ultra Clean Air Unit, India, Mumbai).After solidification of the media, bacteria culture *(*Bacillus and *Escherichia coli)* (50 µl) was spread on the solid surface of the media. Over this inoculated Petri dish, one drop of gel solutions (20 mg /10 ml distilled water) was added using a 10 µl tip and the plates were incubated for 48 h at 37 ^{0}C. After the incubation period, the zone of inhibition (in mm diameter) was observed and tabulated.

2.5.9. Tensile test
The tensile parameters of the SCMC and SCMC SNCF samples were determined using the INSTRON 3369 Universal Testing Machine (Buckinghamshire, England). The specimens with dimensions of length 100 mm and width 10 mm were used. A gauge length of 50 mm was maintained for all the samples. The tensile parameters-maxi-mum stress, modulus and % elongation at break were determined at a crosshead speed of 5 mm/min using a 10 kg load cell. In each case, three samples were used and the average value reported.

2.5.10. Disc method
Nutrient agar medium was prepared by mixing peptone (5.0 g), beef extract (3.0 g), and sodium chloride (NaCl) (5.0 g) in 1000 ml distilled water and the pH was adjusted to 7.0. Finally, agar (15.0 g) was added to the solution. The agar medium was sterilized in a conical flask at a pressure of 15 lbs for 30 min. This medium was transferred into sterilized Petri dishes in a laminar air flow chamber (Microfilt Laminar Flow Ultra Clean Air Unit, India, Mumbai). After solidification of the media, E. coli and bacillus culture was spread on the solid surface of the media. To this inoculated Petri dish, one drop of gel solution (20 mg/10 ml distilled water) was added using 50-ll tip and incubated for 2 days at 37LC in the incubation chamber.

2.5.11. Count method
The effect of bacterial growth of E. coli in mineral salt medium (MSM) was studied in the presence of AgNPs or HSNCs. This medium was prepared by the following composition: NH_4NO_3 (1.5 g), KH_2PO_4 (2.5 g), K_2HPO_4 (0.5 g), NaCl (1.0 g), $MgSO_4$ (1.5 g), $MnSO_4$ (0.01 g), $FeSO_4$ (0.05 g), and $CaCl_2$ (0.05 g) and these were added to 1000 ml of distilled water and the pH was adjusted to 7.0. Then, yeast extract (0.01%) was added for bacterial growth. After that the MSM medium was sterilized, 50 ml of solution was transferred into a sterilized 250-ml conical flask. Afterward, 100 ll E. coli bacterium was added into the media. Finally, 100 ll of Ag-AuNPs solution (20 mg/ 10 ml distilled water) or its equivalent Ag-AuNPs suspension was added, and the optical density of the bacterial medium was measured using a UV–vis spectrophotometer at 600 nm.

2.5.12. Absorbance count method
The effect of bacterial growth of bacillus in mineral salts medium (MSM) was studied in the presence of nanoparticles (Ag, Au, Au-Ag nanoparticles)(28). This medium was prepared by the following composition: NH_4NO_3 (1.5 g), KH_2PO_4 (2.5 g), K_2HPO_4 (0.5 g), NaCl (1.0 g), $MgSO_4$ (1.5 g), $MnSO_4$ (0.01 g), $FeSO_4$ (0.05 g), and $CaCl_2$ (0.05 g) were added to 1000 mL of distilled water and the pH was adjusted to 7.0. Then, yeast extract (0.01%) was added for bacterial growth. After that the MSM medium was sterilized and 50 mL of solution was transferred into a sterilized 250-mL conical flask. Afterward, 100 µL bacillus bacterium was added into the media. Finally, 100 µL of nanoparticles solution (10 mg/5 mL distilled water) or its equivalent nanoparticles suspension was added, and the optical density of the bacterial medium was measured using a UV-vis spectrophotometer at 600 nm.

3. Result and Discussion

3.1 Swelling Properties

The nanoparticle formation depends principally on the swelling behaviour of films. The results in Fig.5.1show that the values of the swelling characteristics were influenced by the films concentration. With an increase in the Hydroxyethyl cellulose (HEC) concentration results in increasing in the swelling ratio values of the bimetallic nanocomposite films due to the hydrophilic nature of HEC. However, bimetallic nanocomposite films have higher swelling ratios, when compared to the conventional HEC films. The reason being due to self reduction, many Ag^+–Au^{3+} are added that led to the formation of the nanocomposite within the films.

Licensed Under Creative Commons Attribution CC BY

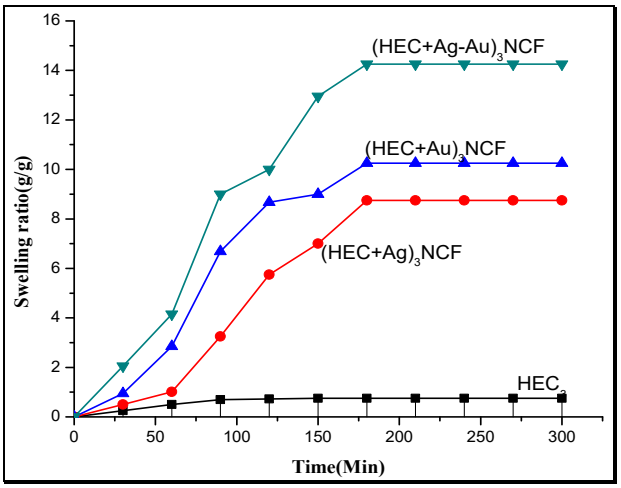


Figure 3.1: Swelling rate of (a) HEC_3 (b) (HEC $+Ag^0)_3$NCF,(c) (HEC $+Au^0)_3$NCF and (d) (HEC $+Ag^0$-$Au^0)_3$NCF

Film code	HEC_3	(HEC-$Ag^0)_3$NCF	(HEC-$Au^0)_3$NCF	(HEC-Ag^0-$Au^0)_3$NCF
Swelling ratio(g/g)	0.75	8.75	10.25	14.25

3.2 Fourier transform infrared (FTIR) spectroscopy analysis

Fig. 5.2 shows the FTIR spectra of HEC_3, single metallic (HEC + $Ag^0)_3$, (HEC+$Au^0)_3$ and dual metallic (HEC+ Ag^0-$Au^0)_3$ nanocomposite films. The spectrum of the HEC films shows a broad absorption band at 3491 cm^{-1} that is related to the asymmetric and –OH symmetric stretching vibrations, the bands at 2935 -2825 cm^{-1} are attributed to stretching vibrations of the $–CH_3$ unit and the absorption band at 1656 cm^{-1} is from the carbonyl groups of the HEC films. The other main characteristic peaks of HEC at 1113-1118 cm^{-1} were assigned to the carbonyl group. However, these peaks shifted in the case of the single metallic (HEC+ $Ag^0)_3$, (HEC+$Au^0)_3$ and dual metallic nanocomposite films (HEC + Ag^0-$Au^0)_3$. Table 2 illustrates the important peaks observed for the single metallic (HEC+$Ag^0)_3$, (HEC+$Au^0)_3$ and dual metallic nanocomposite films (HEC+ $Ag^0)_3$,(HEC+$Au^0)_3$. Overall, the shifting of the peaks confirms the formation of nanoparticles with HEC_3.

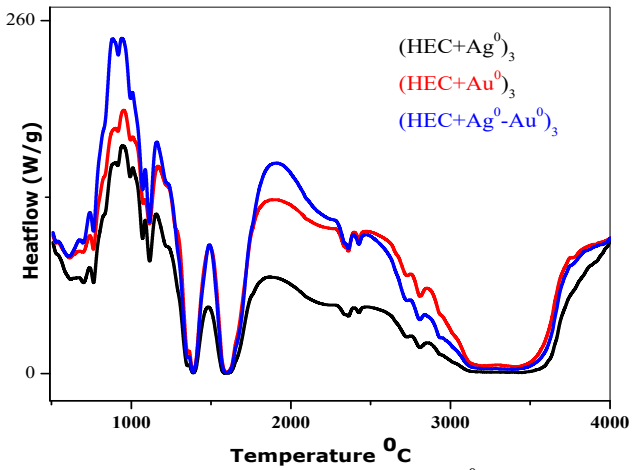


Figure 3.2: FTIR spectra of (a) (HEC + $Ag^0)_3$, (b) (HEC + $Au^0)_3$ and (c) (HEC + Ag^0-$Au^0)_3$ nanocomposite films

Table 2: Fourier transform infrared spectral data of the HEC based films

Film Code	*FTIR bands (cm^{-1})*
(HEC-$Ag^0)_3$	3491, 3128, 2801, 2365, 1603, 1372, 1094, 912, 610
(HEC-$Au^0)_3$	3479, 2825, 2704, 2353, 1590, 1408, 1118, 706
(HEC-Ag^0+ $Au^0)_3$	2935, 2791, 2706, 2426, 1834, 1656, 1579, 1562, 1427, 1325, 1113, 927, 774, 621

3.3 UV–Visible spectroscopy analysis of Ag^0 –Au^0 nanocomposite

The formation of Ag^0 - Au^0 nanoparticles in the films were analyzed by comparing the UV-spectra of metallic and bimetallic nanocomposite solutions (Fig.3.3), formation of silver-gold nanoparticles show a characteristic peak at 417.55 nm. Similarly, UV abortion peaks of Ag^0 and Au^0 nanoparticles were obtained at 549.47 nm, 449.65nm which indicates the formation of both silver as well as gold nanoparticles in the HEC film. The spectral study once again suggests that simultaneous reduction of $HAuCl_4$ and $AgNO_3$ in solution and giving a film containing homogeneous alloy nanoparticles.

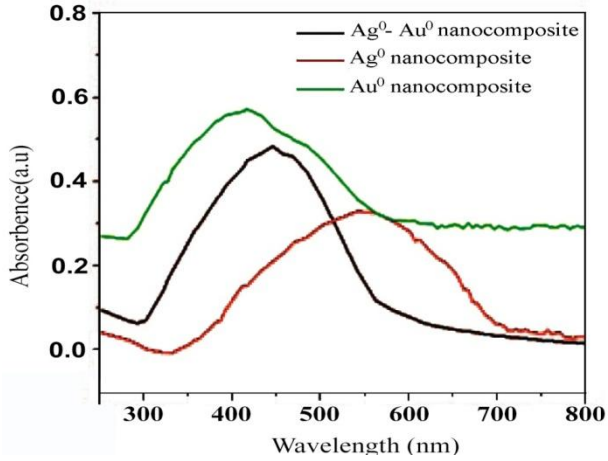


Figure 3.3: UV- Spectrum of nanocomposites (Ag^0, Au^0, and Ag^0-Au^0 nanocomposites)

3.4 Thermogravimetric Analysis (TGA)

Thermogravimetric analysis was used to study the formation of nanoparticles and the thermal stability of the different films. As shown in Fig.3.4 the thermal decomposition of HEC_3 and single metallic (HEC+ $Ag^0)_3$,(HEC+$Au^0)_3$ and bimetallic (HEC + Ag^0- $Au^0)_3$ nanocomposite films occurred at 625 °C with a significant mass loss of 99.81%, 98.12%, 96.59%, respectively. For the bimetallic nanocomposite films (HEC + Ag^0-$Au^0)_3$, a comparatively very low mass loss (96.59%) was observed at 625°C, which was due to the partial decomposition of the Ag^0 and Au^0 nanoparticles. Moreover, according to the TGA results, the bimetallic nanocomposite films (HEC + Ag^0 - $Au^0)_3$ showed a higher thermal stability when compared with the other films.

Licensed Under Creative Commons Attribution CC BY

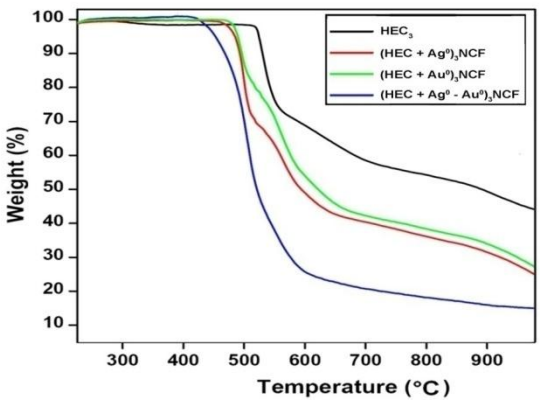


Fig. 3.4 : Thermogravimetric curves of (a) HEC_3 (b) $(HEC+Ag^0)_3NCF$ (c) $(HEC+Au^0)_3NCF$ and (d) $(HEC+Ag^0\text{-}Au^0)_3NCF$

3.5. X-ray diffraction studies

The X-ray diffraction study gives spotting information of nanoparticles formed in the HEC_3 film networks which shows crystalline peaks in Figure 3.5.When compared to the bimetallic nanocomposite blank HEC_3 films does not expose such type of peaks Figure 3.5 (a). However in the case of Ag with Au nanocomposite films can exhibit 2θ highly sharp peaks at 24.24, 38.28, 44.52 and 64.83 when compared to other films, which can be corroborated to (111), (200), (220) and (222) reflections, due to the formation of bimetallic Ag^0 with Au^0 nanocomposite films Figure. 3.5(b).

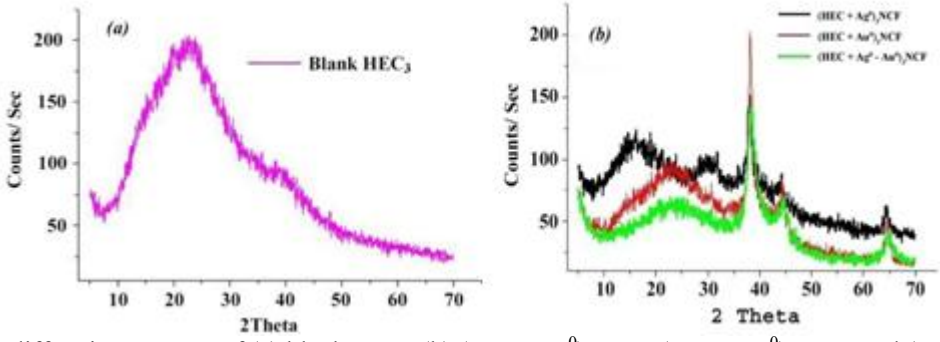


Figure 3.5 : X-ray diffraction patterns of (a) blank HEC_3 (b) $(HEC+Ag^0)_3NCF$, $(HEC+Au^0)_3NCF$, and $(HEC+Ag^0\text{-}Au^0)_3NCF$

3.6 Scanning electron microscopy

The structure and elemental composition of the nanoparticles were investigated by SEM. The film morphology stabilization of dependents on the HEC_3 content (Fig.3.6).Fig. 3.6(a) shows that the dual-metallic loaded nanocomposite film HEC_3 has fewer nanoparticles. Fig.3.6 (b) shows formation of Ag^0 nanoparticles $(HEC+Ag^0)_3$ in NCF, and Fig.3.6(c) shows formation of Au^0 nanoparticles $(HEC+Au^0)_3$ in NCF, it is obvious from Fig.3.6 (d) that a huge quantity of dual-metallic nanoparticles was dispersed on the $(HEC+Ag^0\text{-}Au^0)_3$ in NCF .The same results were confirmed with optical micrograph images of SEM in Fig.3.7.

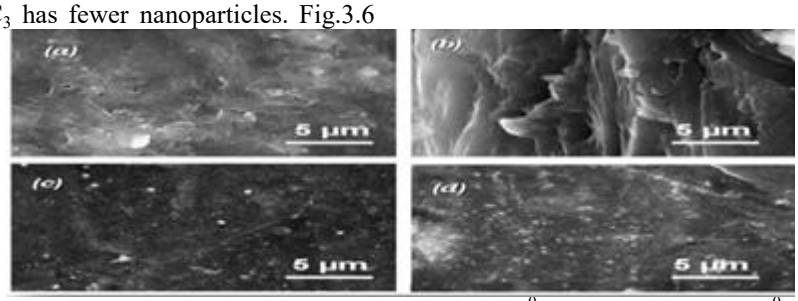


Figure 3.6: Scanning electron micrographs of (a)HEC_3 and (b)$(HEC+Ag^0)_3NCF$, (c) $(HEC+Au^0)_3NCF$ and (d) $HEC+Ag^0\text{-}Au^0)_3NCF$

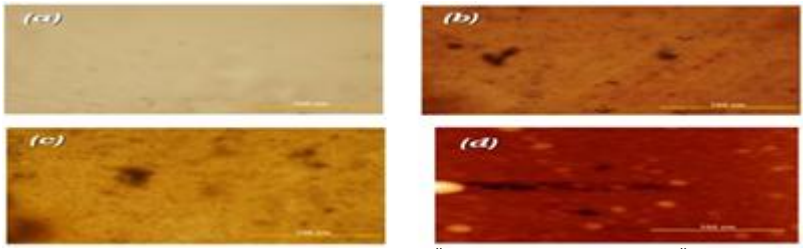


Figure 3.7: Optical micrograph images of (a) HEC_3, (b)$(HEC+Ag^0)_3NCF$, (c) $(HEC+Au^0)_3NCF$ and (d) $HEC+Ag^0\text{-}Au^0)_3NCF$

3.8 Transmission electron microscopy (TEM) analysis

TEM images of Ag^0,Au^0 and bimetallic Ag^0–Au^0 nanoparticles on HEC_3films have an average diameter of ~20nm and their corresponding size distribution of histograms are shown in Fig. 3.8 a, b and c respectively. The images show that all three colloidal nanoparticles have „near monodisperse" size distributions.

Licensed Under Creative Commons Attribution CC BY

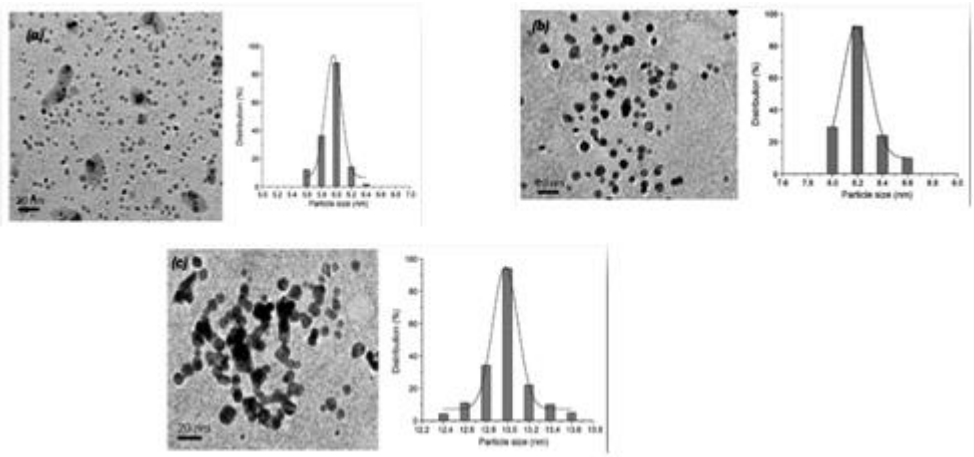


Fig.3.8: Transmission electron images of (a) $(HEC+Ag^0)_3NCF$, (b)$(HEC+Au^0)_3NCF$ and (c) $(HEC+Ag^0\text{-}Au^0)_3NCF$

3.9 Mechanical Properties

Many synthetic and natural polymeric materials are developed to treat the burn wounds and as antibacterial materials. However, they have limited applicability due to poor mechanical properties as well as lower rates of water absorption. A number of hydroxyethyl cellulose bimetallic nanocomposites have been developed for many applications. To have better mechanical strength silver impregnated hydroxyethyl cellulose bimetallic nanocomposites are developed in the present investigation for higher applicability. The mechanical properties of HEC_3 and $(HEC+Ag^0\text{-}Au^0)_3NCF$ films are presented in Table 3. The higher stress at maximum load, modulus, and elongation at break are noticed for $(HEC+Ag^0\text{-}Au^0)_3$ nanocomposite film compared to HEC_3 film.

Table 3: Mechanical properties of HEC and HECNCFs

Sample code	Maximum stress (MPa)	Young"s modulus (MPa)	Elongation at break (%)
HEC_3	12.52	710	1.481
$(HEC+Ag^0)_3$	16.84	1058	2.012
$(HEC+Au^0)_3$	15.21	925	1.658
$(HEC+Ag^0\text{-}Au^0)_3$	18.58	1247	2.241

3.10 Antibacterial property test

Inorganic nanoparticles inherently possess bacteria-killing properties, but by modifying the inorganic nanoparticles these properties can be improved. Recently in the biomedical field, a synthesis of much smaller nanoparticles by a green process was developed to enhance the inactivation of bacteria by „Inhibiting the formation of pits" mechanism. These pits cause polymer molecules and membrane proteins of the bacteria to leak, leading to microbial death. The dual nanoparticles enter into the bacteria cell more effectively, causing damage to the nuclei and resulting in faster bacterial death. The antimicrobial efficacy of the bimetallic hydrogels developed from nanoparticles was examined against Bacillus and E. coli model bacteria. The effects of the HEC_3, $(HEC + Ag^0)_3$, $(HEC + Au^0)_3$ and $(HEC + Ag^0 - Au^0)_3$ films on bacteria are shown in Fig. 3.10.

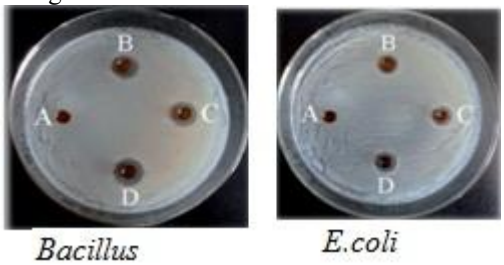


Figure 3.10: Antibacterial activity of (A) HEC_3 (B) $(HEC+Ag)_3NCF$ (C) $(HEC+Au)_3NCF$ (D) $(HEC+Ag\text{-}Au)_3$ NCF against Bacillus, E. coli by disc diffusion method

4. Conclusions

In summary, it is clearly illustrated that the $Ag^0\text{-}Au^0$ nanoparticles are being formed not only on the surface of film but also throughout the networks of hydroxyethyl cellulose. The nanocomposites are analyzed by using spectral, thermal, and electron microscopy methods. They are confirmed as excellent antibacterial materials against Bacillus and Escherichia coli.

The development of synthetic and fabrication technologies for fundamental understanding of nanocomposite films will continue with a greater emphasis on designing sophisticated multi component and complex materials that can be tailored to very specific applications. Emerging new techniques strongly support the systematic characterization of nanocomposite gels which, in return, drives research forward and impacts the rational design of materials.

References

[1] Vigneshwaran,N., Nachane, R. P. , Balasubramanya, R. H. and Varadarajan, P.V., *Carbohydrate Research*, vol. 341, no. 12, (2006), pp. 2012–2018.
[2] Kassaee, M.Z., Akhavan, A., Sheikh, N., and Beteshobabrud, R., Radiation Physics and Chemistry, vol. 77, no. 9, (2008), pp. 1074–1078.
[3] Sharma, V. K., Yngard, R. A. , and Lin, Y., *Advances in* Colloid and Interface Science, vol. 145, no. 1-2,(2009), pp. 83–96.

Licensed Under Creative Commons Attribution CC BY

[4] Valodkar, M., Bhadoria, A., Pohnerkar, J., Mohan, M., and Thakore, S., Carbohydrate Research, vol. 345, no. 12, (2010), pp. 1767–1773.
[5] Hebeish, A., El-Naggar, M.E., G. Fouda, M.M., Ramadan, M.A., Al-Deyab, S.S., and El-Rafie, M.H. *Carbohydrate Polymers*, Vol. 86, No. 2, (2011), pp. 936–940.
[6] El-Rafie, M.H., El-Naggar, M.E., Ramadan, M.A., G. Fouda, M.M., Al-Deyab, S.S., and Hebeish, A., *Carbohydrate Polymers*, vol. 86, no. 2, (2011), pp. 630–635.
[7] Djokovi´c, V., Krsmanovi´c, R., Bo˘zani´c, D. K. et al., Colloids and Surfaces B, Vol. 73, No. 1, (2009), pp. 30–35.
[8] Raveendran, P., Fu, J., and Wallen, S.L., *Green Chemistry*, vol. 8, no.1, (2006) pp.34–38.
[9] Huang, H., Yuan, Q., and Yang, X., "Preparation and characterization of metal-chitosan nanocomposites," *Colloids and Surfaces B*, vol. 39, no. 1-2,(2004), pp. 31–37.
[10] Chen, J., Wang, J., Zhang, X., and Jin, Y *Materials Chemistry and Physics*,vol.108, no. 2-3, (2008), pp. 421–424.
[11] Liu, W., Zhang, Z., Liu, H., He, W., Ge, X., and Wang, M., *Materials Letters*, vol. 61, no. 8-9,(2007), pp. 1801–1804.
[12] Hebeish, A.A., El-Rafie, M.H., Abdel-Mohdy, F.A., Abdel-Halim, E.S. and Emam, H.E., Carbohydrate Polymers, vol. 82, no. 3,(2010), pp. 933–941.
[13] Lu, S., Gao, W., Gu, H.Y., *Burns*, Vol. 34, No. 5, (2005), pp.623-628.
[14] Durango, A.M., Soares, N.F.F., Benevides, S., Teixeira, J., Carvalho, M., Wobeto, C., Andrade, N.J., *Packaging Technology Science*,Vol.19, No.1, (2006), pp.55-59.
[15] Tripathia, S., Mehrotra, G.K., and Dutta, P.K., International Journal of Biological Macromolecules, Vol. 45, No. 4, (2009), pp. 372-376.

Licensed Under Creative Commons Attribution CC BY